Annu. Rev. Biophys. Biomol. Struct. 1999. 28:1–27
Copyright © 1999 by Annual Reviews. All rights reserved

Annu. Rev. Biophys. Biomol. Struct. 1999.28:1-27. Downloaded from www.annualreviews.org
by Harvard University on 01/12/12. For personal use only.

RAMAN SPECTROSCOPY OF PROTEIN AND NUCLEIC ACID ASSEMBLIES

George J. Thomas, Jr.
School of Biological Sciences, University of Missouri-Kansas City, Kansas City, Missouri 64110; e-mail: thomasgj@cctr.umkc.edu

KEY WORDS: structure, dynamics, virus assembly, protein/DNA recognition, telomere

ABSTRACT

The Raman spectrum of a protein or nucleic acid consists of numerous discrete bands representing molecular normal modes of vibration and serves as a sensitive and selective fingerprint of three-dimensional structure, intermolecular interactions, and dynamics. Recent improvements in instrumentation, coupled with innovative approaches in experimental design, dramatically increase the power and scope of the method, particularly for investigations of large supramolecular assemblies. Applications are considered that involve the use of (*a*) time-resolved Raman spectroscopy to elucidate assembly pathways in icosahedral viruses, (*b*) polarized Raman microspectroscopy to determine detailed structural parameters in filamentous viruses, (*c*) ultraviolet-resonance Raman spectroscopy to probe selective DNA and protein residues in nucleoprotein complexes, and (*d*) difference Raman methods to understand mechanisms of protein/DNA recognition in gene regulatory and chromosomal complexes.

CONTENTS

1056-8700/99/0610-0001$08.00

Annu. Rev. Biophys. Biomol. Struct. 1999.28:1-27. Downloaded from www.annualreviews.org
by Harvard University on 01/12/12. For personal use only.

PERSPECTIVES AND OVERVIEW

In the 1928 report of the discovery bearing his name, CV Raman and his collaborator KS Krishnan demonstrated through analysis of perhaps the simplest of biological molecules—H_2O—that the spectrum of inelastically scattered light can provide a unique fingerprint of molecular structure (69). In the intervening 70 years, the scope and versatility of Raman scattering spectroscopy have improved in many ways. A diverse family of Raman-related mechanisms has been discovered, and many are applicable to large proteins and nucleic acids and their assemblies. Novel experimental approaches continue to be developed for increasingly complex biological systems, including enzyme-substrate complexes, chromatin, viruses, membrane assemblies, and whole cells.

The focus of this review is on recent developments that facilitate the use of Raman spectroscopy to obtain information of the following types from nucleoprotein assemblies: (*a*) conformation or orientation of constituent molecules and submolecular groups, (*b*) local hydrogen-bonding interactions, and (*c*) time dependence of structural or organizational properties. Typically, this information cannot be obtained by other structure-determining methods, such as X-ray or nuclear magnetic resonance (NMR) analysis, either because of the large sizes of the assemblies or as a consequence of limitations inherent in the alternative probes.

The present review is intended to complement recent surveys of biomolecular Raman applications, which cover the following specific areas in much greater detail: Raman and resonance Raman spectroscopy of nucleic acids (64, 86, 90), Raman and resonance Raman spectroscopy of proteins (3, 39, 54, 77, 88), Raman tensor determinations (92), Raman microspectroscopy of cells and cellular components (35, 68), and Raman spectroscopy in biomedicine (47, 56). The reader is referred also to more general treatments of the theory and practice of Raman and resonance Raman spectroscopy as they relate to the study of biological molecules (18, 55).

NATURE OF THE DATA OF RAMAN SPECTROSCOPY

Underlying Principles and General Considerations

In applications to condensed phases, the Raman scattering spectrum provides essentially the same type of information as the infrared (IR) absorption spectrum,

Annu. Rev. Biophys. Biomol. Struct. 1999.28:1-27. Downloaded from www.annualreviews.org
by Harvard University on 01/12/12. For personal use only.

namely, the energies of molecular normal modes of vibration. However, the two methods differ fundamentally in mechanism and selection rules, and each has specific advantages and disadvantages for biological applications (55). Instrumentation is typically more complex for Raman (light scattering) than for IR (light absorption); also Raman data collections are generally slower and more tedious, often leading to signal-to-noise levels inferior to those obtainable by modern Fourier-transform IR (FTIR) methods. Additionally, it is problematic to compare quantitatively the scattering intensities of Raman bands, whereas IR absorption intensities are governed by Beer's Law. Conversely, water is a notoriously strong IR-absorbing medium, and aqueous systems cannot be investigated with ease by IR methods. In contrast, water (H_2O or D_2O) interferes only feebly with Raman spectra of aqueous solutions and hydrated solids. Indeed, samples of virtually any hydration level can generally be investigated more favorably by Raman than by IR spectroscopy.

A fundamental difference in selection rules leads to another important advantage of Raman over IR for the study of large molecules and assemblies. For a localized molecular vibration to generate a Raman band, there must be an associated change in polarizability, i.e. a distortion of electron density in the vicinity of the vibrating nuclei. Thus, localized vibrations of multiply bonded or electron-rich groups (C=O, C=N, C=C, S−S, S−C, S−H, etc) generally produce more intense Raman bands than do vibrations of singly bonded or electron-poor groups. Accordingly, the Raman spectrum of a protein is largely dominated by bands associated with the peptide main chain, aromatic side chains, and sulfur-containing side chains. (Note that, although aliphatic and other nonaromatic side chains generate comparatively weak Raman bands, their large numbers in a protein can cumulatively produce a significant contribution to certain regions of the Raman spectrum, as noted below.) For similar reasons, the Raman spectrum of a nucleic acid is dominated primarily by bands caused by vibrations localized either within the heterocyclic bases or in backbone phosphate groups. In contrast, IR absorption intensities depend on an oscillating dipole moment with vibration, and therefore vibrations of all types of nonsymmetrically bonded atoms can contribute substantially to the IR spectrum. Thus, IR absorption spectra of proteins and nucleic acids, more so than Raman spectra, are complicated by overlapping bands from many types of residues. These considerations explain the greater spectral simplicity of the Raman signature vis-à-vis the IR signature of a typical biomolecule, which in turn simplifies spectral band measurements and structural interpretations.

Other notable advantages of Raman spectroscopy are (*a*) applicability to samples in different physical states (solutions, suspensions, precipitates, gels, films, fibers, single crystals, amorphous solids, etc) and to large macromolecular assemblies, (*b*) a spectroscopic timescale ($\sim 10^{-14}$ s) that is short in comparison with either biomolecular structure transformations or protium/deuterium

exchanges, (*c*) nondestructiveness of data collection protocols, (*d*) minimal requirements of sample mass (∼1 mg) and volume (∼1 μL), (*e*) no requirement for chemical labels or probes, and (*f*) existence of a large database of Raman spectra of model compounds for which reliable band assignments, normal mode analyses, and spectra-structure correlations have been made. The correlations are generally transferable to proteins and nucleic acids and facilitate interpretation of spectra.

Annu. Rev. Biophys. Biomol. Struct. 1999.28:1-27. Downloaded from www.annualreviews.org
by Harvard University on 01/12/12. For personal use only.

Raman Frequencies, Intensities, and Polarizations

The discrete vibrational energies (Raman band frequencies), scattering probabilities (Raman intensities), and tensor characteristics (Raman polarizations) that constitute the Raman spectrum are a unique and sensitive function of molecular geometry and intra- and intermolecular force fields. In a typical experiment, the spectrum is excited by a laser, such as the green line of the argon laser at 514.5 nm (or 19,436 cm^{-1} in wavenumber units), and measured by recording the intensities of bands that are 500–1800 cm^{-1} lower than the laser excitation wavenumber. This region of the spectrum contains virtually all of the fundamental vibrational information on a protein or nucleic acid molecule, except for hydrogenic stretch modes, which generate bands in the 2400–3600 cm^{-1} Raman interval. For example, the Raman frequency corresponding to the sulfhydryl (S−H) bond stretch of a cysteinyl side chain occurs in the 2500–2600 cm^{-1} interval. When the group of vibrating atoms in the macromolecule is sufficiently small and identifiable, as is the case for the cysteine S−H bond stretch, the vibration is referred to as a group vibration and its Raman band is designated a group frequency. For both proteins and nucleic acids, many group frequencies have been identified and their assignments supported by normal coordinate calculations (3, 54, 55, 64, 86, 87, 90). Figure 1 illustrates the complete Raman vibrational spectrum of a large nucleoprotein complex, the icosahedral double-stranded DNA (dsDNA) bacteriophage P22. The legend indicates details of sample conditions and identifies representative Raman bands that are diagnostic group frequencies of the viral capsid subunit and packaged dsDNA genome.

Polarization is a useful characteristic of Raman scattered light. Although the incident laser beam is plane polarized, the Raman scattered light is not generally polarized in the same plane. The change of polarization for randomly oriented molecules is defined quantitatively by the depolarization ratio $\rho \equiv I_\perp/I_\parallel$, the quotient of scattered intensities along directions perpendicular ($I_\perp$) and parallel ($I_\parallel$) to the direction of incident-light polarization. In isotropic ensembles (solutions), measurements of ρ are helpful in distinguishing normal modes of vibration that are totally or locally symmetric (i.e. which retain the symmetry of the molecule or subgroup and for which $\rho < 0.75$) from those

Annu. Rev. Biophys. Biomol. Struct. 1999.28:1-27. Downloaded from www.annualreviews.org
by Harvard University on 01/12/12. For personal use only.

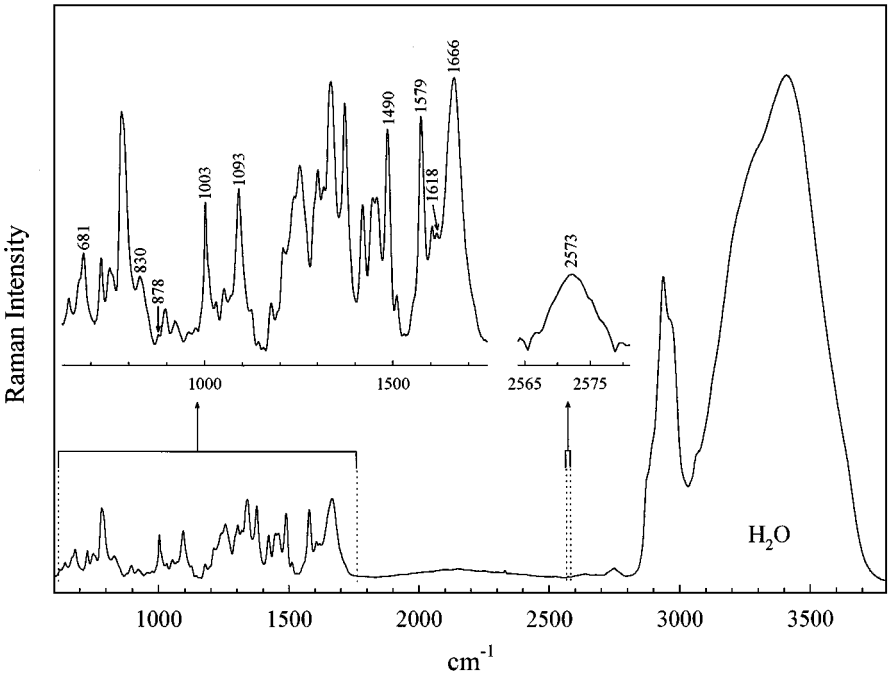

Figure 1 Raman spectrum (514.5 nm excitation) of P22 virus at 80 μg/μL in H_2O buffer (10 mM Tris, 200 mM NaCl, 10 mM $MgCl_2$, pH 7.5) at 20°C; sample volume, 2 μL; no smoothing of data. Bottom trace shows the complete spectrum, including H_2O solvent (3000–3700 cm^{-1}) and aliphatic C–H stretch modes of viral protein and DNA (~2900 cm^{-1}). Most structurally informative Raman bands occur in the 600–1800 cm^{-1} interval, expanded in the upper trace. Labels indicate representative Raman markers of dG (681 cm^{-1}), DNA backbone (830 and 1093 cm^{-1}), Trp (878 cm^{-1}), Phe (1003 cm^{-1}), dA and dG (1490 and 1579 cm^{-1}), Tyr and Trp (1618 cm^{-1}), and protein amide I (1666 cm^{-1}). Also labeled is the S–H stretch (2573 cm^{-1}), informative of the environment and dynamics of Cys 405 of the capsid subunit. Note that the 2573 cm^{-1} band is a marker of roughly one of every 20,000 bonds in the virion.

modes that are not ($\rho = 0.75$). In anisotropic ensembles, such as oriented single crystals and fibers, appropriate measurement of polarized Raman intensities (see below) can yield detailed information on orientations of molecules and their subgroups. Experimental techniques required for measurement of Raman polarizations of crystals and fibers are described in detail elsewhere (92).

Nonresonance and Resonance Raman Spectra

The spectrum of Figure 1 was obtained under nonresonance conditions (off-resonance), meaning that the excitation wavelength (514.5 nm) is well separated

from wavelengths of electronic absorption of viral protein and nucleic acid molecules. If, on the other hand, the excitation wavelength is chosen to be within a region of protein or DNA electronic absorption (<300 nm), then a resonance Raman spectrum would be obtained. Selection rules governing resonance Raman and off-resonance Raman transitions differ fundamentally from one another, and consequently the intensities of Raman bands observed in the two types of spectra can be quite different (3, 18, 54, 55, 58, 90). In brief, a resonance Raman spectrum will exhibit Raman bands only from the chromophore in resonance, because resonance Raman scattering probabilities (intensities) are many orders of magnitude greater than those of off-resonance Raman scattering. As an example, Figure 2 compares Raman spectra of the filamentous virus fd (600–1800 cm^{-1} region) obtained using excitations that are off-resonance (514.5 nm) and in resonance with either DNA base absorptions (257 nm) or protein tryptophan and tyrosine absorptions (229 nm). Thus, whereas the 514.5-nm spectrum exhibits a rich pattern of Raman bands from all viral components, the 229-nm excitation produces Raman signatures only of residues Trp 26, Tyr 21, and Tyr 24 of the coat protein subunit, and 257-nm excitation produces a spectrum dominated by Raman signatures of DNA bases of the packaged single-stranded DNA (ssDNA) genome. Because the latter two spectra are excited in the ultraviolet (UV), they are referred to as UV-resonance Raman (UVRR) spectra. Further discussion of UVRR excitation profiles of nucleic acid and protein constituents is given elsewhere (37, 90).

DEVELOPMENTS IN INSTRUMENTATION AND EXPERIMENTAL DESIGN

In the past few years, instrumentation for Raman spectroscopy has changed dramatically, reflecting improved design of laser light sources, optical filters, and photon detectors. Powerful and stable continuous-wave lasers are now commercially available for Raman excitations extending from the near IR to the UV. Long-wavelength Raman excitation offers the significant advantage over shorter-wavelength excitation of greater freedom from potentially interfering fluorescence of target molecules or trace contaminants. For UV wavelengths, laser technology has improved to the point that collection of UVRR spectra of nucleoprotein complexes, including virus assemblies, is now feasible. Advent of the holographic notch filter to more effectively reject elastically scattered (Rayleigh) light, introduction of the axial transmissive grating to maximize photon throughput, and implementation of efficient charge-coupled-device detectors also have contributed to dramatic increases in spectrophotometric sensitivity and selectivity. State-of-the-art Raman spectrometer systems have been

Annu. Rev. Biophys. Biomol. Struct. 1999.28:1-27. Downloaded from www.annualreviews.org
by Harvard University on 01/12/12. For personal use only.

Annu. Rev. Biophys. Biomol. Struct. 1999.28:1-27. Downloaded from www.annualreviews.org
by Harvard University on 01/12/12. For personal use only.

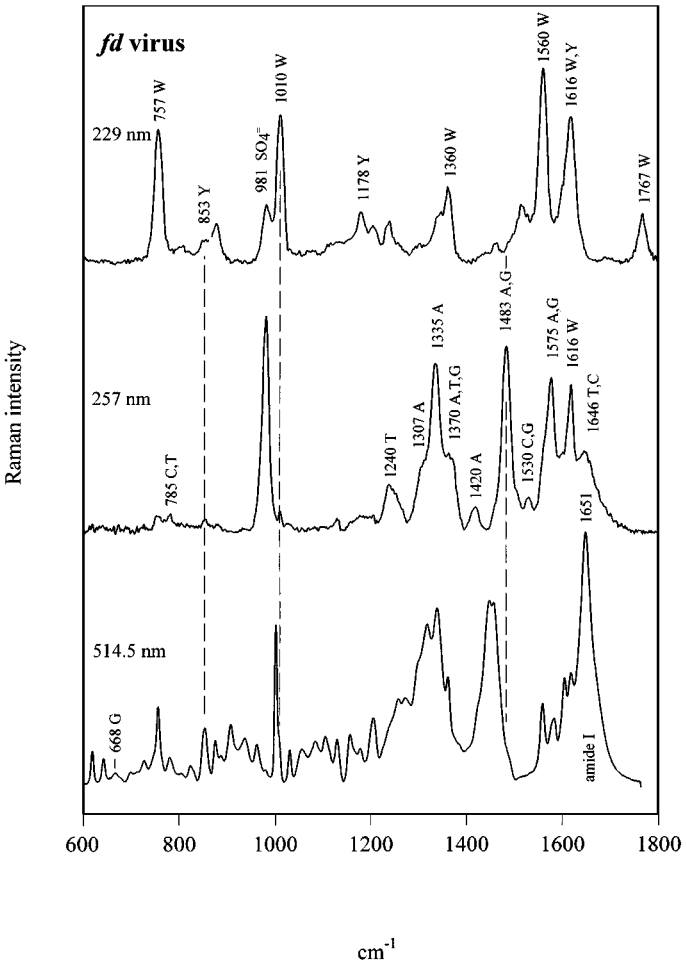

Figure 2 Raman spectra (600–1800 cm^{-1}) of fd virus excited at 514.5 nm (*bottom*, 50 $\mu g/\mu L$), 257 nm (*middle*, 0.5 $\mu g/\mu L$), and 229 nm (*top*, 0.5 $\mu g/\mu L$). Data illustrate the complementary nature of off-resonance (514.5 nm) and UVRR (257 and 229 nm) excitations. Off-resonance excitation produces a rich pattern of Raman bands, primarily from viral coat subunits, which constitute about 88% of the virion mass. The strongest band, amide I at 1651 cm^{-1}, is diagnostic of subunit α-helix; the weak band at 668 cm^{-1} identifies C3′-*endo*/*anti* dG in packaged DNA; neither band appears in UVRR spectra. The spectrum excited at 257 nm is the Raman signature primarily of packaged ssDNA bases, as labeled. The spectrum excited at 229 nm is the Raman signature of coat protein Trp and Tyr, as labeled (2, 59–62, 97). No smoothing of data was performed.

described for biological applications of UVRR (1, 36, 73), near-IR Raman (15, 29), Raman optical activity (5, 6, 57), and confocal Raman microscopy (24, 34, 76).

Among technical innovations in Raman sample cell design and laser illumination, those that facilitate either temporal or spatial resolution of biomolecular phenomena are particularly valuable. In principle, time-resolved Raman spectroscopy can span a wide temporal domain, from tens of femtoseconds ($\sim 10^{-14}$–10^{-13} s, representing periods of typical group frequencies) to indefinitely long periods. Spiro and coworkers have demonstrated that intermediates with lifetimes as short as tens of nanoseconds ($\sim 10^{-8}$ s) can be characterized along the relatively rapid R → T allosteric pathway of hemoglobin by using pulse-probe resonance Raman techniques (38, 71). Detailed reviews of subpicosecond applications have been given by Kincaid (39) and by Spiro & Czernuszewicz (77). Slower structural transformations that characterize the maturation of large protein assemblies, such as viral capsids, may be time-resolved by using flow dialysis sampling methods (19, 45, 95). The latter technology is also particularly useful for measurement of hydrogen-isotope exchanges to probe solvent-accessible surfaces of proteins and nucleic acids (70).

Three-dimensional structure information may be culled from Raman spectra of biomolecules provided that two key conditions are met. First, the target molecules must be of uniform and known orientation with respect to the electric vector of the exciting laser beam, and second, Raman scattering tensors for the diagnostic Raman bands must be known beforehand. (A unique Raman tensor, which relates electric vectors of incident and scattered light in the local coordinate system, determines the intensity and polarization of each Raman band.) The first criterion can be satisfied for appropriately oriented single crystals or fibers; the second requires tedious polarized Raman measurements on suitable model structures (9, 82, 89). A Raman microscope facilitates this experimental approach, which is described in detail elsewhere (92). On a larger scale, multidimensional Raman imaging has recently been reported for polytene chromosomes and human leukemic erythroblasts (76).

A useful tool in the approaches to molecular recognition is the technique of digital difference Raman spectroscopy, developed independently in several laboratories during the early 1980s for efficient spectroscopic characterizations of conformational changes in biomolecules (72). Many interesting applications of Raman difference spectroscopy in studies of biomolecular structure have been reviewed previously (17, 81). The technique is particularly powerful in combination with residue-specific stable-isotope substitutions (2) and site-specific mutagenesis (59). Several recent applications are reviewed below.

Annu. Rev. Biophys. Biomol. Struct. 1999.28:1-27. Downloaded from www.annualreviews.org
by Harvard University on 01/12/12. For personal use only.

Annu. Rev. Biophys. Biomol. Struct. 1999.28:1-27. Downloaded from www.annualreviews.org
by Harvard University on 01/12/12. For personal use only.

APPLICATIONS TO PROTEIN AND NUCLEIC ACID ASSEMBLIES

Representative recent investigations, primarily from the author's laboratory, that provide new information on structure or assembly mechanisms of viruses and nucleoprotein complexes are surveyed here.

Icosahedral Capsid Assembly

The assembly of an icosahedral viral shell from identical protein subunits requires highly specific interactions to sequester hydrophobic residues at subunit interfaces and avert unproductive aggregations. A plausible assembly mechanism is one involving several discrete steps, each with attendant changes in subunit structure. In this scheme, an assembly intermediate (precursor shell or procapsid) would consist of subunits in incompletely folded states, whereas the mature shell (capsid) would contain the most stable subunit fold. Because assembly intermediates are likely to possess subunits of well-defined secondary and tertiary structures, resembling the late-folding intermediates observed for small globular proteins, they should be distinguishable by the extent of protection of their peptide NH groups against deuterium exchange. Although measurement of protium/deuterium (H/D) exchanges in small globular proteins is feasible by NMR spectroscopy (4), icosahedral viral shells typically contain hundreds of large protein subunits and are well beyond the size limitations of NMR methods. An example is the *Salmonella* bacteriophage P22, for which the icosahedral ($T = 7$) capsid comprises 420 copies of a 429-residue (47-kDa) subunit (66). The native virion packages a linear dsDNA genome of 43 kilobase pairs. Recent developments in time-resolved Raman spectroscopy offer a new approach for monitoring H/D exchanges in such assemblies (70, 95, 96). Changes in secondary structure involving as few as 2% of residues can be measured accurately and interpreted structurally by use of this method, which relies on precise monitoring of Raman amide I and amide III bands and their deuterated counterparts, amide I′ and amide III′ (67, 93).

Tuma et al (94) compared Raman amide I, amide III, amide I′, and amide III′ signatures of the precursor procapsid and mature capsid of P22 virus to monitor the nature and extent of peptide H/D exchanges as a function of subunit folding and shell maturation. Electron cryomicroscopy shows that shell maturation involves extensive rearrangements in the surface lattice, with a significant increase ($\sim$10%) in shell radius and pronounced angularization of icosahedral vertices (Figure 3, top panel). Nevertheless, Raman spectroscopy identifies only a small change in subunit secondary structure ($\sim$2.5%) accompanying shell maturation, despite extensive changes in side-chain environments (67). Together, these

Annu. Rev. Biophys. Biomol. Struct. 1999.28:1-27. Downloaded from www.annualreviews.org
by Harvard University on 01/12/12. For personal use only.

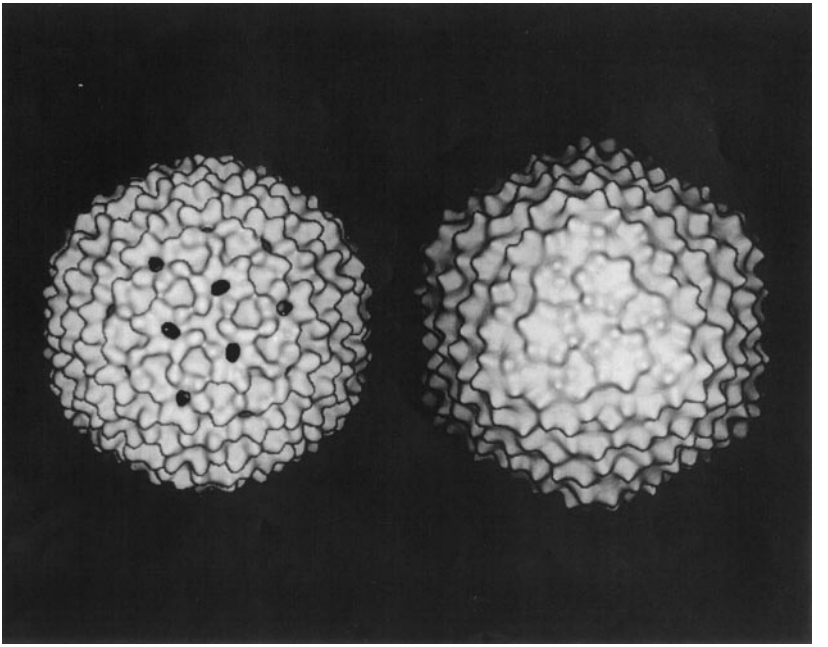

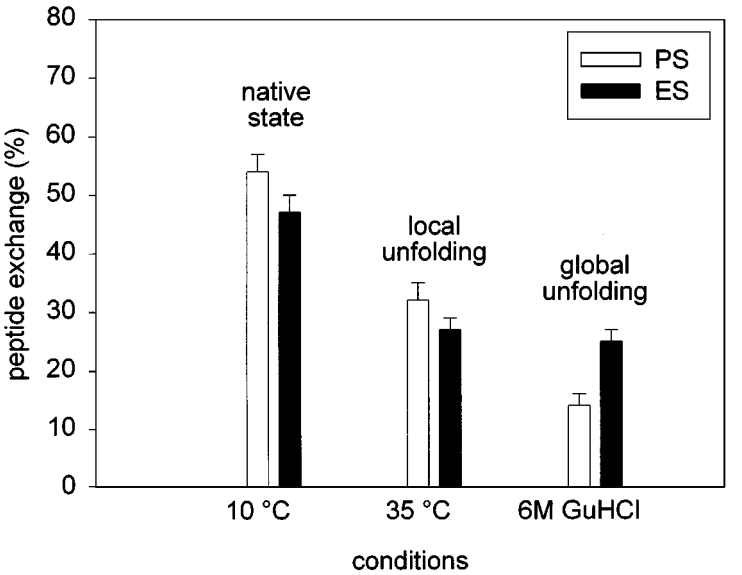

findings suggest that domain movement involving hinge bending mediates the shell transformation. Amide exchange protection, determined by the Raman dynamic probe for three distinct subunit states of both precursor and mature shells (94), is compared in the bottom panel of Figure 3. The data confirm the proposed molecular mechanism by demonstrating a large increase—nearly twofold—in the exchange-protected subunit core of the mature shell vis-à-vis that in the precursor shell.

Further insight into this mechanism is obtained by examining Raman markers of specific side chains in procapsid and expanded shells (94). As shown in the top panel of Figure 4, the single cysteine (Cys 405) sulfhydryl of the shell subunit generates its Raman SH marker (S−H bond stretching vibration) at 2569 cm^{-1} in the procapsid, but at 2573 cm^{-1} in the mature capsid, indicating that the procapsid SH donates a significantly stronger hydrogen bond (44). The SH Raman marker also serves as a valuable probe of local dynamics. Thus, the bottom panel of Figure 4 shows that SH → SD exchange of Cys 405 is slower in the procapsid shell than in the expanded shell and is characterized in the former by a relatively large Arrhenius activation energy for local unfolding ($E_a^{local} =$ 44 kcal · mol^{-1}) (94). When this result is compared with measurements of the global activation energy for shell expansion in the physiological temperature range ($E_a^{global} =$ 35–40 kcal · mol^{-1} at 37°C), it can be concluded further that opening of one SH-containing interface is sufficient to trigger shell expansion. The proposed mechanism is depicted schematically in Figure 5 (94).

The striking increase in subunit H/D exchange protection accompanying expansion of the P22 shell (Figure 3, bottom) implies a corresponding increase in close packing of hydrophobic side chains, similar to a protein-folding event. Thus, subunits of the precursor and mature shells may be regarded as representing, respectively, a late-folding intermediate and the final native state of the shell subunit. In this context, the native conformation, i.e. the state of lowest free energy, is attained only within the expanded shell (Figure 5, bottom panel). Such coupling of folding and assembly has been proposed (94) as a general pathway for the construction of supramolecular complexes.

←

Figure 3 Top panel: Reconstructions of the P22 procapsid shell (*left*) and mature capsid shell (*right*) from electron-cryomicroscopic images. Maturation leads to expansion (∼10% increase in diameter) of the shell, filling of channels in the shell lattice, and angularization of icosahedral vertices. (From PE Prevelige, Jr, unpublished data; see also reference 65). Bottom panel: Comparison of amide exchange protection of the P22 procapsid shell (PS) and the expanded shell (ES), as determined by a Raman dynamic probe of three distinct subunit states in each assembly: native state (*left*), locally unfolded state (*middle*), and globally unfolded state (*right*) that exposes the exchange protected core (94). Expansion leads to moderate decreases in amide exchanges of native and locally unfolded states, but a very large (nearly twofold) increase in the exchange-protected core.

Annu. Rev. Biophys. Biomol. Struct. 1999.28:1-27. Downloaded from www.annualreviews.org
by Harvard University on 01/12/12. For personal use only.

Annu. Rev. Biophys. Biomol. Struct. 1999.28:1-27. Downloaded from www.annualreviews.org
by Harvard University on 01/12/12. For personal use only.

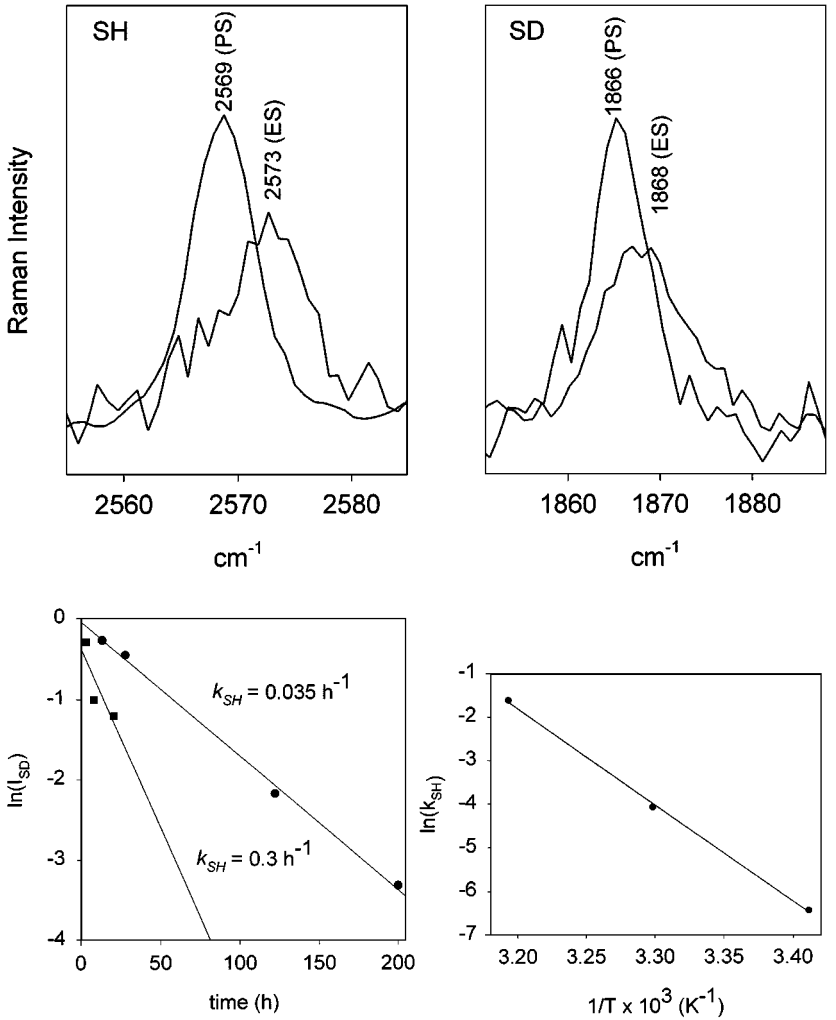

Figure 4 Top panel: Raman SH (*left*) and SD (*right*) markers of Cys 405 in subunits of the procapsid shell (PS) and the expanded shell (ES). The shift with expansion of the SH marker from 2569 to 2573 cm^{-1} (or that of the SD marker from 1866 to 1868 cm^{-1}) signifies a weaker SH (or SD) hydrogen bond donor in the expanded shell (44). Raman accessibility to both the SH and SD bands (in H_2O and D_2O solutions, respectively) facilitates time resolution of the SH → SD reaction. Bottom panel: Time-resolved rates of sulfhydryl exchange (k_{SH}) of Cys 405 in subunits of the procapsid shell at 30°C (*circles*) and the expanded shell at 2°C (*squares*). Data (*left*) were obtained by measuring the intensity decay of the Raman SH marker of the shell as a function of time of exposure to D_2O. For the procapsid shell, the data yield an Arrhenius plot (*right*) with slope corresponding to an activation energy for local unfolding (E_a^{local}) of 44 kcal · mol^{-1}. (From reference 94.)

Annu. Rev. Biophys. Biomol. Struct. 1999.28:1-27. Downloaded from www.annualreviews.org
by Harvard University on 01/12/12. For personal use only.

Mechanisms of viral DNA packing (2, 70) and nucleosomal DNA condensation (25, 26, 31–33) have also been investigated by similar implementations of Raman difference spectroscopy.

Filamentous Virus Architecture

Bacteriophage fd is a flexible filament of ~6-nm width and ~880-nm length, comprising a coat of approximately 2700 50-residue α-helical subunits (83) and encapsidating a small circular ssDNA genome (~6400 bases). Although the detailed structure is not known, assembly models have been proposed on the basis of genetics studies, fiber X-ray diffraction, and spectroscopic measurements (reviewed in 48). Because ssDNA constitutes only a small percentage (12%) of the virion mass, the mode of DNA interaction with coat protein subunits has been difficult to assess. Fiber X-ray diffraction studies provide no direct evidence on the structure of the packaged genome, DNA base environments, coat protein side-chain orientations, or intersubunit interactions. However, these issues can be addressed by Raman, and UVRR methods, and numerous studies have been reported in recent years (2, 50, 59–63, 80, 83–85, 91, 97). Here we consider the use of methods based on polarized Raman measurements, which yield detailed structural information on constituents of the native virus assembly.

Overman et al (63) examined oriented fibers of fd in a Raman microscope and determined the intensities of Raman scattering in directions parallel (cc) and perpendicular (bb) to the virion axis. (The raw data are similar to those in the off-resonance Raman spectrum of fd shown in Figure 2.) With knowledge of the amide I Raman tensor, transferred from the crystal structure of the model amide aspartame (89), the polarized Raman amide I intensity ratio, I_{cc}/I_{bb}, could be related to the average angle (θ) by which the axis of the α-helical coat protein subunit is tilted from the virion axis (63), i.e. $I_{cc}/I_{bb} = (4)(0.537\sin^2\theta + \cos^2\theta)^2/(0.537\cos^2\theta + \sin^2\theta + 0.537)^2$. The measured value, $I_{cc}/I_{bb} = 3.01\ (\pm 0.18)$, yielded $\theta = 16^\circ\ (\pm 3^\circ)$, where the uncertainty reflects experimental error. Effects of imperfect virion orientation were also considered. Estimates of θ from model-building studies compare favorably with the experimentally determined value.

Tsuboi et al (91) used a similar polarized Raman approach to investigate the side-chain orientation of the unique and essential tryptophan residue (Trp 26) of the fd coat subunit in the native virion. With knowledge of Raman tensors for the key tryptophan markers at 1340 (normal mode W7′), 1364 (W7), and 1560 (W3) cm^{-1}, the Eulerian coordinates (θ, χ) of the Trp 26 side chain were determined. The plane of the indole ring (θ) was found to be nearly parallel to the virion axis ($0 \pm 10^\circ$), whereas the indolyl pseudo-twofold axis (χ) was found to be directed at an angle of $36 \pm 3^\circ$ to the virion axis. It is important to note that these results are completely independent of any assumed assembly

Annu. Rev. Biophys. Biomol. Struct. 1999.28:1-27. Downloaded from www.annualreviews.org
by Harvard University on 01/12/12. For personal use only.

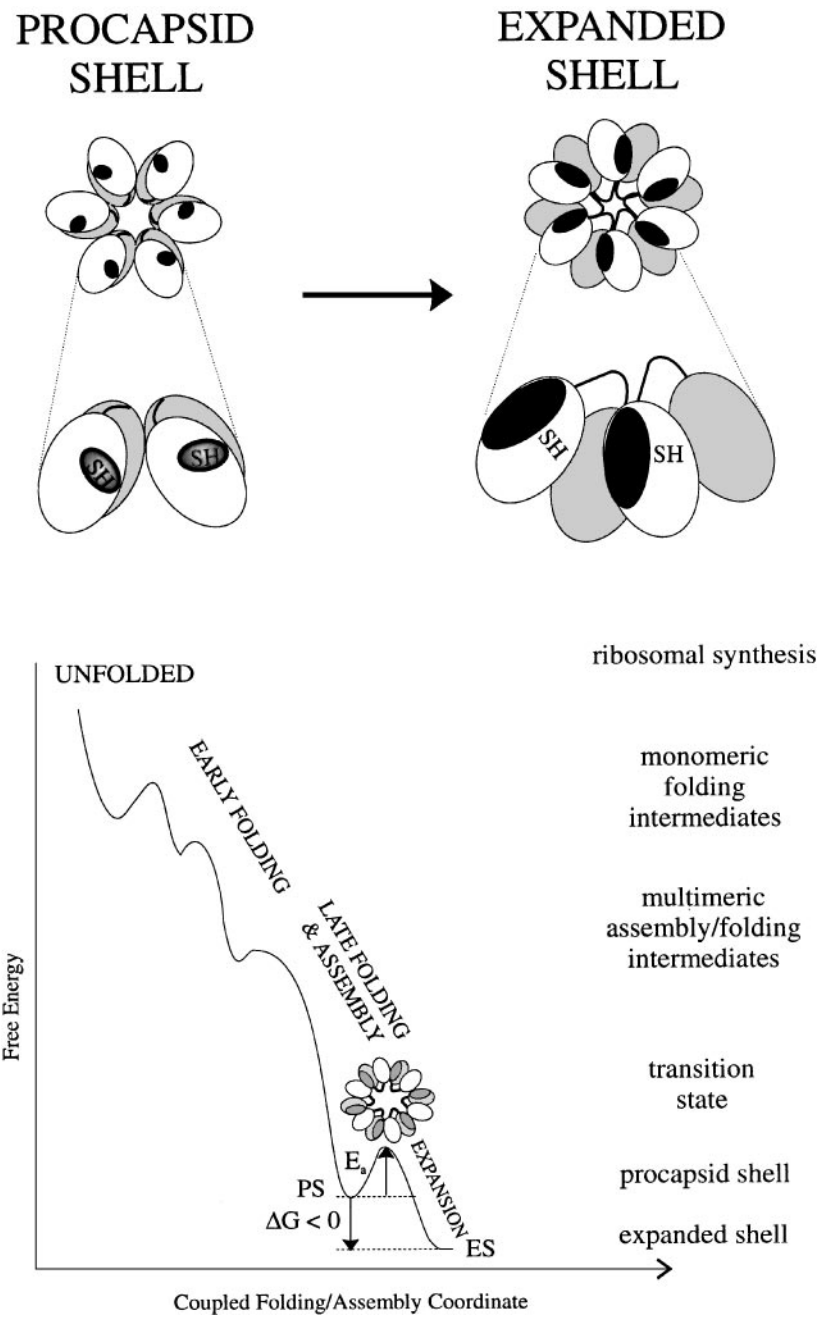

Annu. Rev. Biophys. Biomol. Struct. 1999.28:1-27. Downloaded from www.annualreviews.org
by Harvard University on 01/12/12. For personal use only.

model. When combined with the Raman-determined value for the side-chain torsion $\chi^{2,1}$ (2) and energy minimized (16) in the context of the Marvin assembly model (Protein Data Bank, identification code 1IFJ), the structure depicted in Figure 6 is obtained. Interestingly, the Raman-based structure (Figure 6) differs significantly from the original 1IFJ model in that the indole ring is directed more toward the subunit C terminus than toward the N terminus.

An alternative Raman-based method for determining residue orientation has been developed recently by Takeuchi and coworkers (50, 80), who used a novel velocity gradient flow cell to orient fd virions unidirectionally in solution. In this approach, UVRR excitation was used to select for Raman bands of the chromophore in resonance with a single molecular electronic transition, which constitutes the basis for structural interpretation of the observed Raman anisotropy (Raman linear intensity difference or RLID). Studies of fd with 266- and 240-nm excitations (raw data similar to those in the UVRR spectra of fd shown in Figure 2) have provided independent determination of the Trp-26 orientation, in substantial agreement with Figure 6. The RLID measurements additionally support the small α-helix tilt angle and suggest a plausible scheme for ssDNA packaging in the virion (80). In a more recent RLID study of mutant filamentous virions, in which the two subunit tyrosines of the coat subunit were independently mutated to methionine (Y21M and Y24M), the tyrosine side-chain orientations were determined for the first time (50). The results show that the twofold axis of the phenolic ring (C1–C4 line) of Tyr 21 is inclined at $39.5 \pm 1.4^\circ$ from the virion axis, whereas that of Tyr 24 is inclined at $43.7 \pm 0.6^\circ$. The orientation determined for Tyr 21 is close to that of the Marvin model (1IFJ). However, the orientation determined for Tyr 24 differs from the 1IFJ model by a 40° rotation about the Cα-Cβ bond. The RLID results suggest plausible neighbors for tyrosine side chains in the virion assembly and indicate highly hydrophobic environments for aromatic rings of both Tyr 21 and Tyr 24, as previously proposed on the basis of off-resonance Raman investigations (59).

←

Figure 5 Top: A mechanism accounting for the observed effective increase in the exchange-protected core of subunits of the P22 procapsid shell (*left*) upon maturation to the expanded shell (*right*), represented here as domain interchange between neighboring subunits. In the upper portions of both cartoons, the lattices of the shells are represented as clusters of six subunits (hexons), in which the subunit exchange-protected core is indicated by black shading and putative mobile domains are shown as unshaded and lightly shaded. The lower portions of both cartoon enlargements depict Cys 405 sulfhydryls and rearrangements of contacts and domains between two neighboring subunits. Bottom: Energy-landscape representation of coupling between subunit folding and capsid assembly in P22. A transition state containing partially exposed hydrophobic surfaces (*dark grey*) is proposed for the heat-induced expansion (94).

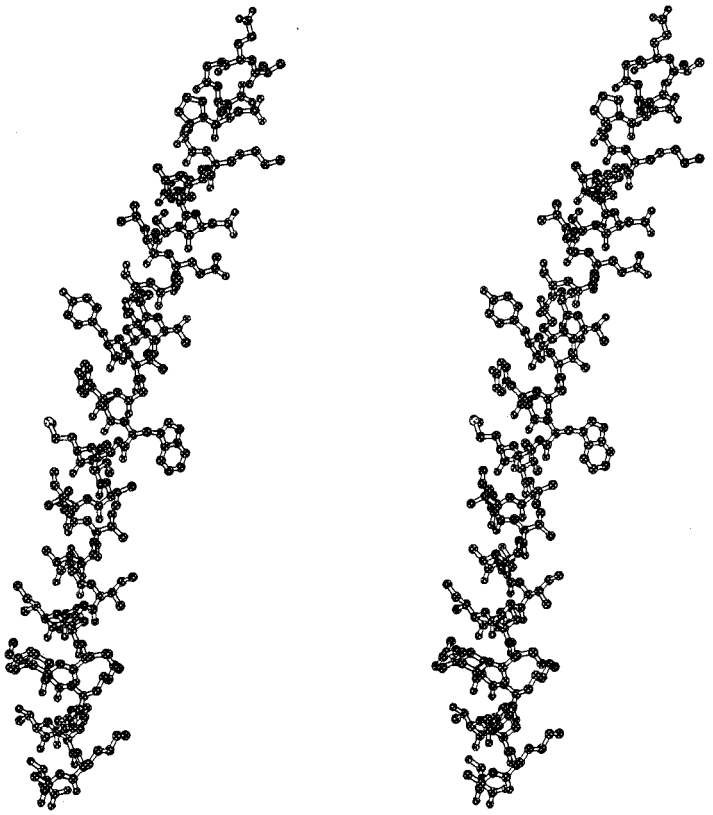

Figure 6 Stereo diagram of an energy-minimized (16) structural model for the native fd subunit, based on indole ring orientation obtained from polarized Raman microspectroscopy of oriented fibers (91), Trp 26 side-chain torsion $\chi^{2,1}$ indicated by the Raman W3 mode (2), average helix tilt angle of 16° with respect to the virion axis determined by polarized Raman microspectroscopy (63), and virion symmetry from fiber X-ray diffraction (49, 79). The virion axis runs vertically. Molecular graphics generated by MOLSCRIPT (40).

Annu. Rev. Biophys. Biomol. Struct. 1999.28:1-27. Downloaded from www.annualreviews.org
by Harvard University on 01/12/12. For personal use only.

Protein/DNA Recognition in Gene Regulatory Complexes

Interactions of proteins with DNA regulate gene transcription, replication, and recombination events. Protein-DNA interactions are also important in chromosomal condensation and packaging phenomena. Although structural details of many protein-DNA complexes have been revealed by single-crystal X-ray and solution NMR investigations (46, 78), much remains to be learned about the underlying mechanisms. One difficulty with high-resolution structure methods has been the limited availability of both protein-bound and -unbound structures

Annu. Rev. Biophys. Biomol. Struct. 1999.28:1-27. Downloaded from www.annualreviews.org
by Harvard University on 01/12/12. For personal use only.

of the same DNA target site. Raman spectroscopy is not impeded in this respect and is potentially of great value to complement X-ray and NMR methods as a probe of protein-DNA recognition. Raman spectra of protein-DNA complexes can be obtained over a wide range of experimental conditions, including those approximating in vivo assembly pathways. The Raman vibrational signature of DNA is also highly sensitive to conformational reorganizations induced by both specific (12) and nonspecific (8) protein binding.

In a series of studies from our laboratory (7, 8, 10–14), Raman signatures were identified for activators of transcription that bind specifically to the DNA major groove (wild-type and mutant cI repressors of phage λ, Ner repressor of phage D108, and the bZIP protein GCN4 of yeast) and minor groove (hSRY-HMG box). Nonspecific ssDNA-binding (gene V protein of phage M13) has also been characterized. In conjunction with available X-ray structures of protein-DNA complexes, the Raman band perturbations have been correlated with protein-induced DNA reorganization. The structural perturbations induced by protein binding are illustrated in Figure 7 for representative complexes in the form of Raman difference spectra (Raman difference profiles between each complex and its constituents). These data demonstrate that the degree of DNA structural perturbation is directly correlated with the extent to which DNA is deformed by the protein under conditions of optimal binding. Many novel Raman band perturbations have been revealed in these studies, and they provide a rich database for continuing evaluation of biologically significant protein-DNA recognition. One example of immediate interest is the extraordinarily prolific difference spectrum of the hSRY-HMG:DNA complex (Figure 7, bottom), which reflects protein-induced expansion of the minor groove, bending of the DNA double helix toward the major groove, and, importantly, a putative diagnostic fingerprint of bent DNA (14).

Telomeric DNA Polymorphism

A eukaryotic telomere—the end of a linear chromosome—consists typically of an adenine- and cytosine-rich 3′ strand paired to a guanine- and thymine-rich 5′ strand, the latter with tandem repeats of its telomeric GT motif extending beyond the end of the 3′ strand. In vivo, the overhanging telomeric repeat is associated with one or more specifically bound proteins (telomere-binding proteins) and may be involved in unusual conformational switching between Watson-Crick duplex and Hoogsteen quadruplex structures (74, 75). Repeats of the telomeric motif of the ciliate *Oxytricha nova* [$d(TTTTGGGG)_n$] represent particularly convenient target sequences for Raman investigation. Miura and coworkers developed a detailed assignment scheme for the fourfold repeat, $d(T_4G_4)_4$ (or Oxy4), demonstrating its structural polymorphism in solution as a function of temperature and ionic composition (52), and time-resolved the

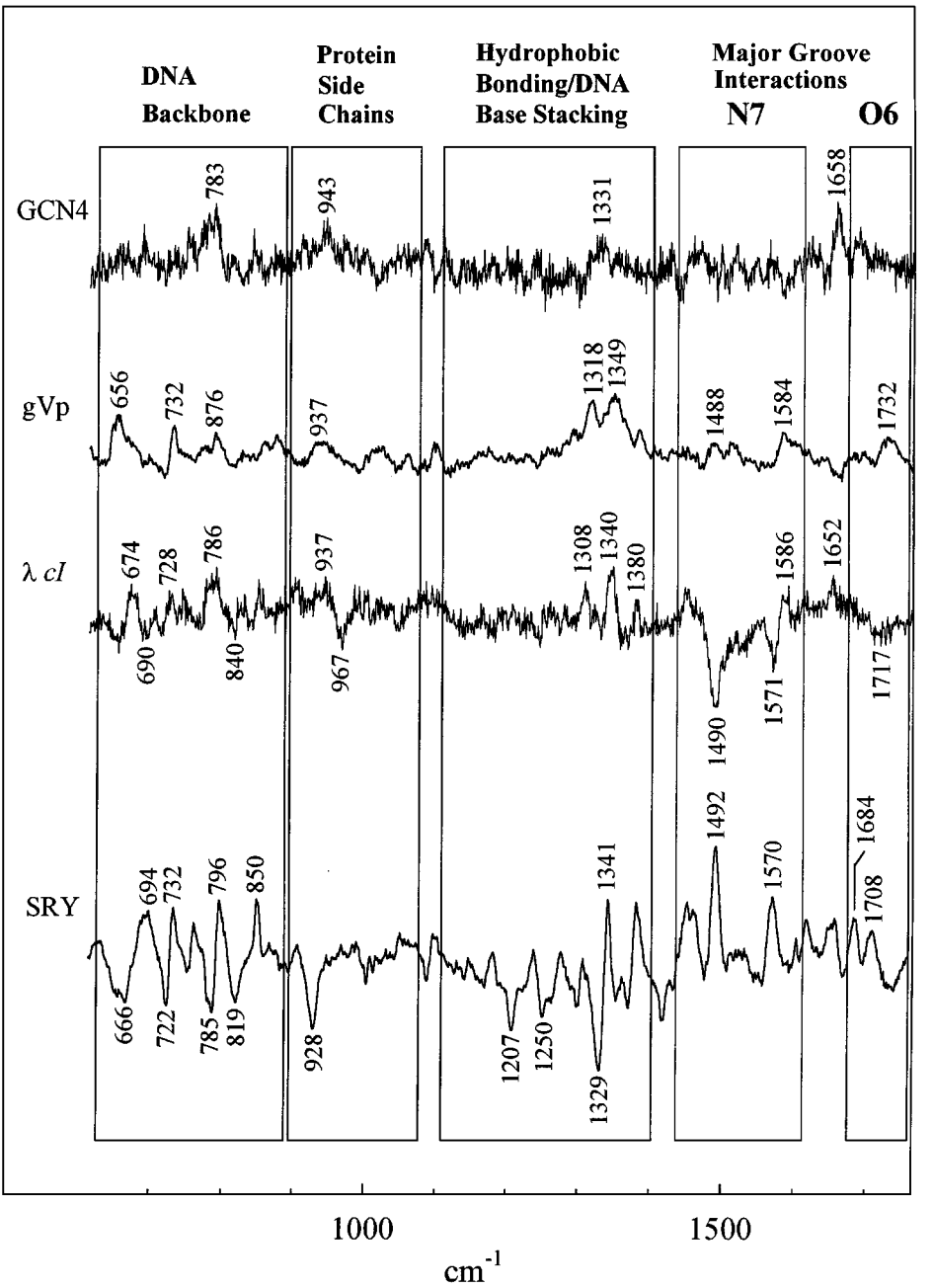

Annu. Rev. Biophys. Biomol. Struct. 1999.28:1-27. Downloaded from www.annualreviews.org
by Harvard University on 01/12/12. For personal use only.

Annu. Rev. Biophys. Biomol. Struct. 1999.28:1-27. Downloaded from www.annualreviews.org
by Harvard University on 01/12/12. For personal use only.

dynamics of guanine imino-NH exchange in Hoogsteen G quartets (53). Additionally, they established a phase diagram for conformational switching between antiparallel-foldback and parallel-extended quadruplex structures (51). Representative data are shown in Figure 8. An important byproduct of these studies has been an enriched database of Raman markers of dG and dT deoxynucleoside conformations and Hoogsteen N7 hydrogen-bonding interaction.

The above studies also provide a background for Raman investigation of the *Oxytricha* telomere-binding protein, a heterodimer comprising 56-kDa (α) and 41-kDa (β) subunits, and the specificity of subunit interactions with the cognate telomeric repeat, $d(T_4G_4)_2$ (41, 43). The results show that the β subunit binds to both $d(T_4G_4)_2$ (Oxy2) and $dT_6(T_4G_4)_2$ (T6Oxy2), but promotes the formation of a parallel-stranded quadruplex only in T6Oxy2, demonstrating the importance of a telomeric 5′ leader for recognition and guanine quadruplex formation. Although Oxy2 is not a suitable substrate for quadruplex promotion by the β subunit, the Raman spectra revealed other structural rearrangements of this DNA strand upon β-subunit binding, including changes in guanine glycosyl torsion angles from syn to anti and disruption of carbonyl hydrogen-bonding interactions. The conformation of Oxy2 in the β:Oxy2 complex was suggested as a plausible intermediate along the pathway to formation of the parallel-stranded quadruplex. A model for β-subunit binding by *Oxytricha* telomeric DNA sequences and a mechanism for quadruplex formation were proposed. A key feature of this model is the use of a novel telomeric hairpin secondary structure as the recognition motif (Figure 9) (41). Subsequent Raman, H/D exchange, and gel mobility studies of Oxy2 and T6Oxy2 provide supporting evidence for a hairpin structure stabilized by G · G pairs (42).

Interactions between the *Oxytricha* α subunit and sequences containing the telomeric repeat (Oxy2 and T6Oxy2) have also been investigated by Raman spectroscopy (43). The α subunit binds specifically and stoichiometrically to the T6Oxy2 hairpin and alters its secondary structure by inducing conformational changes in the 5′ leading sequence (T6) without extensive disruption of G · G pairing. On the other hand, binding of α to Oxy2 completely eliminates G · G pairing and unfolds the hairpin. DNA unfolding is accompanied

←

Figure 7 Raman difference spectra reflecting DNA reorganization caused by different DNA-binding proteins. From top to bottom: The bZIP protein GCN4 binding to an AP1 target site (13); ssDNA-binding protein of M13 phage (gVp) binding to the ssDNA analog, poly(dA) (8); *cI* repressor of phage λ binding to its O_L1 target site (10–12); human sex-determining factor hSRY-HMG box binding to its DNA target site (14). The DNA Raman signature is minimally perturbed by GCN4 and maximally perturbed by hSRY-HMG. The latter result is considered diagnostic of protein-induced large-scale reorganization of the 8-base-pair target site, d(GAACAATC) · d(GATTGTTC), including sharp bending toward the major groove.

Annu. Rev. Biophys. Biomol. Struct. 1999.28:1-27. Downloaded from www.annualreviews.org
by Harvard University on 01/12/12. For personal use only.

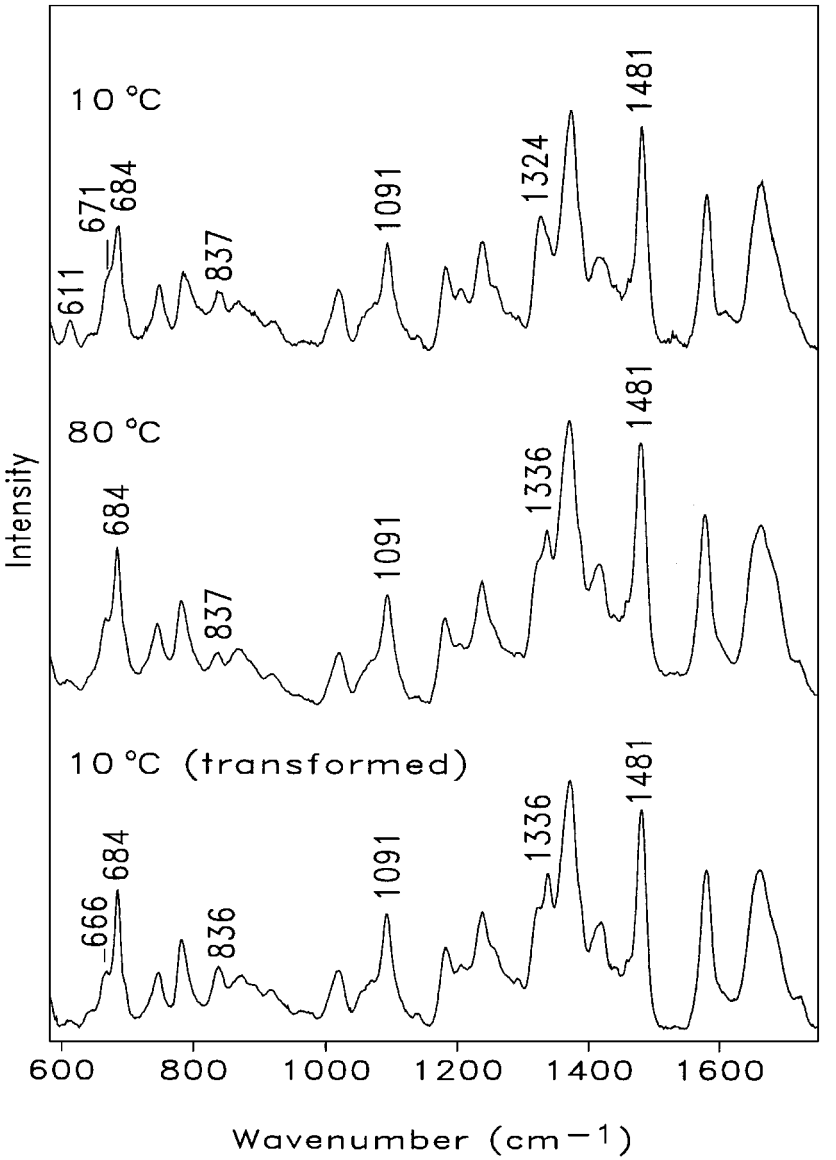

Figure 8 (*Continued*)

Annu. Rev. Biophys. Biomol. Struct. 1999.28:1-27. Downloaded from www.annualreviews.org
by Harvard University on 01/12/12. For personal use only.

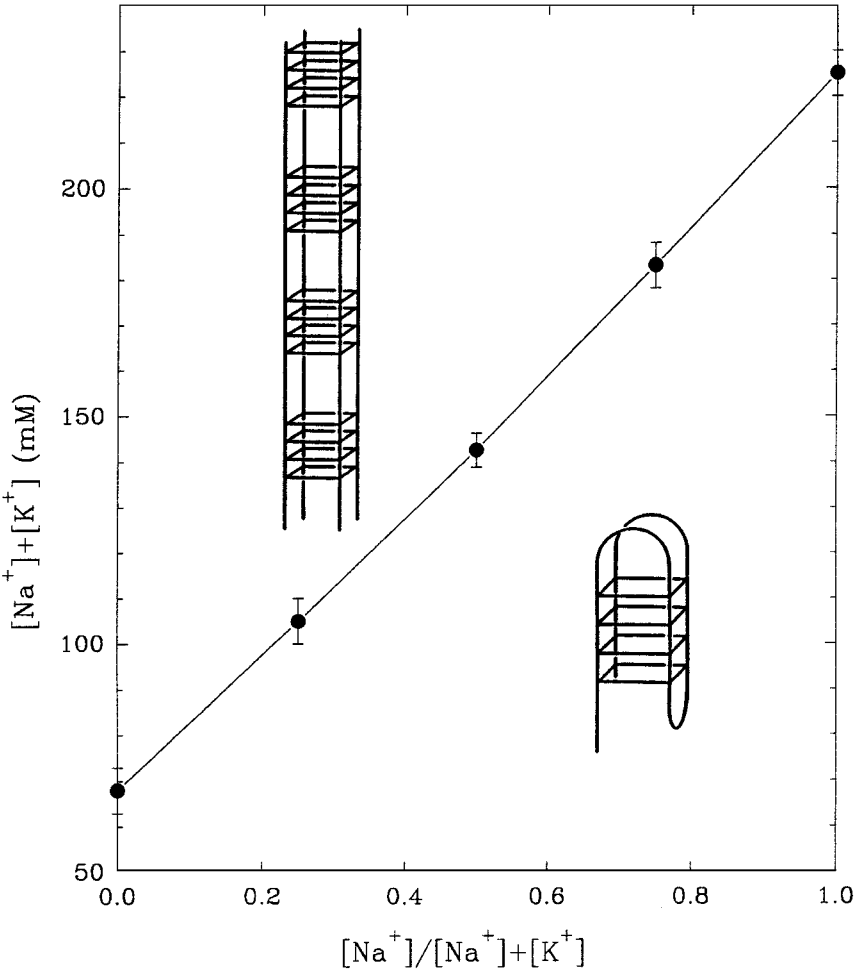

Figure 8 Left panel: Temperature dependence of the Raman spectrum of the *Oxytricha* telomeric repeat Oxy4 (2 mM in 500 mM NaCl, pH 7.0) (52). The initial 10°C spectrum (*top*) is a fingerprint of the antiparallel foldback quadruplex, which is transformed irreversibly to the parallel extended quadruplex at 80°C (*middle*), such that upon subsequent cooling to 10°C the transformed structure is retained (*bottom*). Changes in dG Raman markers, 671 → 666 cm^{-1} and 1324 → 1336 cm^{-1}, signal the structure transformation. The antiparallel structure is also distinguished by a more prominent dT marker near 611 cm^{-1}. Both structures contain a sharp band at 1481 cm^{-1} signaling strong N7 hydrogen bonding (Hoogsteen G-quartets). Right panel: Phase diagram governing polymorphism in solutions of 2.0 mM Oxy4 as determined by Raman spectroscopy (51). The low-salt and high-salt forms are, respectively, the antiparallel foldback and parallel extended quadruplexes, as indicated.

Annu. Rev. Biophys. Biomol. Struct. 1999.28:1-27. Downloaded from www.annualreviews.org
by Harvard University on 01/12/12. For personal use only.

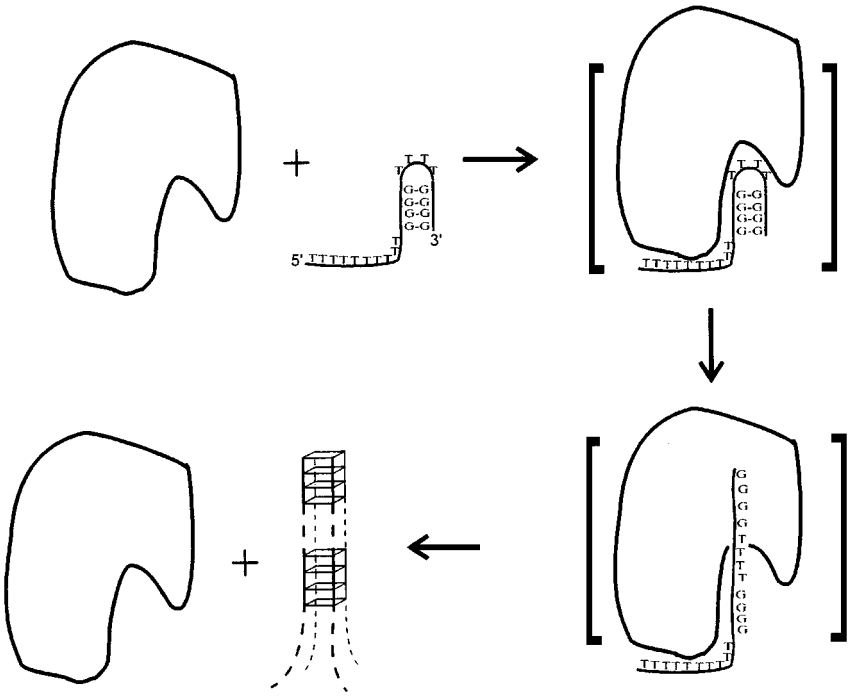

Figure 9 Model for the hairpin-to-quadruplex transformation induced in an *Oxytricha* telomeric repeat (T6Oxy2) by the β subunit of the telomere-binding protein. In this model, a telomeric hairpin is proposed as the DNA recognition motif for the β subunit (*upper left*). The telomeric hairpin is stabilized by G · G base pairs and contains both *syn*- and *anti*-dG conformers. Although stoichiometry is undetermined, a 1:1 complex is assumed for simplicity. Upon binding, G · G pairs are ruptured and the hairpin is destabilized in favor of a single strand containing only *anti*-dG conformers (*lower right*). Telomeric single strands subsequently associate to form the extended parallel quadruplex, stabilized by hydrogen-bonded G quartets (*parallelogram symbols*) separated by runs of T (*dashed lines*) (*lower left*).

by conformational changes affecting both the phosphodiester backbone and dG residues. Interestingly, the α subunit also forms complexes with the non-telomeric isomers $d(TG)_8$ and $dT_6(TG)_8$, evidenced by altered electrophoretic mobility in nondenaturing gels; however, Raman and CD spectra indicate no significant DNA conformational changes. Similarly, the α subunit binds to but does not appreciably alter the secondary structure of duplex DNA. Thus, although the α subunit has the capacity to bind to Watson-Crick and different non-Watson-Crick motifs, DNA refolding is specific to the *Oxytricha* telomeric hairpin, and retention of G · G pairing is specific to the telomeric sequence incorporating the 5′ leader.

Annu. Rev. Biophys. Biomol. Struct. 1999.28:1-27. Downloaded from www.annualreviews.org
by Harvard University on 01/12/12. For personal use only.

Enzyme Mechanisms

Recently, Callender and coworkers have exploited sensitive Raman difference methods in combination with stable-isotope substitutions to characterize changes in bond parameters attendant with binding of transition-state analogues at active sites of adenosine deaminase (28) and ribonuclease A (27).

Carey and colleagues have also developed Raman difference methods in conjunction with isotope substitutions to gain insights into the effects of different active-site environments on proteolysis in serine (21) and cysteine proteases (20, 30). Implementation of these approaches by long-wavelength Raman excitation (752 nm) offers promise that the active-site chemistry of previously problematic flavin-containing enzymes (p-hydroxybenzoate hydroxylase and riboflavin-binding protein) will prove tractable to Raman spectroscopy (22, 23). Importantly, these investigators also point out that state-of-the-art technology now enables the collection of protein Raman spectra off-resonance with acceptable signal-to-noise levels by using sample concentrations in the 100-μM range (29). This is equivalent to a few micrograms per microliter for the typical protein and greatly extends both the number of proteins and types of structural problems that can be addressed by Raman spectroscopy. (Indeed, examination of the raw data of Figure 1, for which signal-to-noise ratios (S:N) exceed 100:1, indicates that viral concentrations of a few micrograms per microliter would yield acceptable S:N values for the more prominent bands of the 600–1800 cm^{-1} interval.)

CONCLUSIONS

Recent developments in instrumentation and sample-handling procedures have vastly improved the sensitivity and selectivity of Raman spectroscopy as a probe of proteins, nucleic acids, and their complexes. Both nonresonance and resonance Raman approaches are now feasible as probes of structure and dynamics in large supramolecular assemblies. With suitable experimental techniques and reliable spectroscopic assignments, these probes can be exploited to investigate orientations of molecular subgroups in native biomolecules, the nature and strength of hydrogen-bonding interactions that function in biomolecular recognition, the kinetic and thermodynamic parameters governing structural transformations in biological assemblies, and molecular images of biomaterials.

ACKNOWLEDGMENT

Support of the National Institutes of Health (Grants GM50776 and GM54378) is gratefully acknowledged.

Visit the *Annual Reviews home page* at http://www.AnnualReviews.org

Annu. Rev. Biophys. Biomol. Struct. 1999.28:1-27. Downloaded from www.annualreviews.org
by Harvard University on 01/12/12. For personal use only.

Literature Cited

1. Asher SA, Bormett RW, Chen XG, Lemmon DH, Cho N, et al. 1993. UV resonance Raman spectroscopy using a new cw laser source: convenience and experimental simplicity. *Appl. Spectrosc.* 47:628–33
2. Aubrey KL, Thomas GJ Jr. 1991. Raman spectroscopy of filamentous bacteriophage *Ff* (*fd, M13, f1*) incorporating specifically-deuterated alanine and tryptophan side chains. *Biophys. J.* 60:1337–49
3. Austin JC, Jordan T, Spiro TG. 1993. Ultraviolet resonance Raman studies of proteins and related model compounds. In *Advances in Spectroscopy (Biomolecular Spectroscopy)*, ed. RJH Clark, RE Hester, 20A:55–127. New York: Wiley & Sons. 383 pp.
4. Bai Y, Selsnick TR, Mayne L, Englander SW. 1995. Protein folding intermediates: native-state hydrogen exchange. *Science* 269:192–97
5. Barron LD, Hecht L. 1994. Vibrational Raman optical activity: from fundamentals to biochemical applications. In *Circular Dichroism, Principles and Applications*, ed. K Nakanishi, N Berova, RW Woody, pp. 179–215. New York: VCH Publ.
6. Barron LD, Hecht L, Bell AF, Wilson G. 1996. Recent developments in Raman optical activity of biopolymers. *Appl. Spectrosc.* 50:619–29
7. Benevides JM, Kukolj G, Autexier C, Aubrey KL, DuBow MS, Thomas GJ Jr. 1994. Secondary structure and interaction of phage *D108* Ner repressor with a 61-base-pair operator: evidence for altered protein and DNA structures in the complex. *Biochemistry* 33:10701–10
8. Benevides JM, Terwilliger TC, Vohník S, Thomas GJ Jr. 1996. Raman spectroscopy of the *Ff* gene V protein and complexes with poly(dA): nonspecific DNA recognition and binding. *Biochemistry* 35:9603–9
9. Benevides JM, Tsuboi T, Bamford JHK, Thomas GJ Jr. 1997. Polarized Raman spectroscopy of double-stranded RNA from bacteriophage ϕ6: local Raman tensors of base and backbone vibrations. *Biophys. J.* 72:2748–62
10. Benevides JM, Weiss MA, Thomas GJ Jr. 1991. Design of the helix-turn-helix motif: nonlocal effects of quaternary structure in DNA recognition investigated by laser Raman spectroscopy. *Biochemistry* 30:4381–88
11. Benevides JM, Weiss MA, Thomas GJ Jr. 1991. DNA recognition by the helix-turn-helix motif: investigation by laser Raman spectroscopy of the phage λ repressor and its interaction with operator sites O_L1 and O_R3. *Biochemistry* 30:5955–63
12. Benevides JM, Weiss MA, Thomas GJ Jr. 1994. An altered specificity mutation in the λ repressor induces global reorganization of the protein-DNA interface. *J. Biol. Chem.* 269:10869–78
13. Benevides JM, Weiss MA, Olson WK, Thomas GJ Jr. 1999. Protein-directed DNA structure I. Raman spectroscopy of a leucine zipper and bZIP complex. *Biochemistry.* In press
14. Benevides JM, Weiss MA, Olson WK, Thomas GJ Jr. 1999. Protein-directed DNA structure II. Raman spectroscopy of a high-mobility-group box with application to human sex reversal. *Biochemistry.* In press
15. Brennan JF III, Wang Y, Ramachandra RD, Feld MS. 1997. Near-infrared Raman spectrometer systems for human studies. *Appl. Spectrosc.* 51:201–08
16. Brünger AT. 1992. *X-PLOR* Version 3.1. New Haven: Yale Univ.
17. Callender R, Deng H. 1994. Nonresonance Raman difference spectroscopy: a general probe of protein structure, ligand binding, enzymatic catalysis, and the structures of biomacromolecules. *Annu. Rev. Biophys. Biomol. Struct.* 23:215–45
18. Carey PR. 1982. *Biochemical Applications of Raman and Resonance Raman Spectroscopies*. New York: Academic. 262 pp.
19. Carey PR. 1996. Want to exchange your virus? Try microdialysis and Raman. *Biophys. J.* 71:2918–19
20. Carey PR. 1998. Raman spectroscopy in enzymology: the first 25 years. *J. Raman Spectrosc.* 29:7–14
21. Carey PR, Tonge PJ. 1995. Unlocking the secrets of enzyme power. *Acc. Chem. Res.* 28:8–13
22. Clarkson J, Jaffe EK, Petrovich RM, Dong J, Carey PR. 1997. Opportunities for probing the structure and mechanism of porphobilinogen synthase by Raman spectroscopy. *J. Am. Chem. Soc.* 119:11556–57
23. Clarkson J, Palfey BA, Carey PR. 1997. Probing the chemistries of the substrate and flavin ring system of *p*-hydroxybenzoate hydroxylase by Raman difference spectroscopy. *Biochemistry* 36:12560–66
24. de Grauw CJ, Otto C, Greve J. 1997. Line-scan Raman microspectrometry for biological applications. *Appl. Spectrosc.* 51: 1607–12
25. Deng H, Bloomfield VA, Benevides JM, Thomas GJ Jr. 1999. Characterization of

Annu. Rev. Biophys. Biomol. Struct. 1999.28:1-27. Downloaded from www.annualreviews.org
by Harvard University on 01/12/12. For personal use only.

genomic DNA structures by Raman spectroscopy. *Biophys. J.* In press
26. Deng H, Bloomfield VA, Benevides JM, Thomas GJ Jr. 1998. Raman spectroscopy of DNA-polyamine complexes. *Biophys. J.* In press
27. Deng H, Burgner JW II, Callender R. 1998. Structure of the ribonuclease · uridine-vanadate transition state analogue complex by Raman difference spectroscopy: mechanistic implications. *J. Am. Chem. Soc.* 120:4717–22
28. Deng H, Kurz LC, Rudolph FB, Callender R. 1998. Characterization of hydrogen bonding in the complex of adenosine deaminase with a transition state analogue: a Raman spectroscopic study. *Biochemistry* 37:4968–76
29. Dong J, Dinakarpandian D, Carey PR. 1998. Extending the Raman analysis of biological samples to the 100 micromolar concentration range. *Appl. Spectrosc.* 52:1117–22
30. Doran JD, Carey PR. 1996. α-Helix dipoles and catalysis: absorption and Raman spectroscopic studies of acyl cysteine proteases. *Biochemistry* 35:12495–502
31. Duguid JG, Bloomfield VA, Benevides JM, Thomas GJ Jr. 1993. Raman spectroscopy of DNA-metal complexes. I. Interactions and conformational effects of the divalent cations: Mg, Ca, Sr, Ba, Mn, Co, Ni, Cu, Pd and Cd. *Biophys. J.* 65:1916–28
32. Duguid JG, Bloomfield VA, Benevides JM, Thomas GJ Jr. 1995. Raman spectroscopy of DNA-metal complexes. II. The thermal denaturation of DNA in the presence of Sr^{+2}, Ba^{+2}, Mg^{+2}, Ca^{+2}, Mn^{+2}, Co^{+2}, Ni^{+2} and Cd^{+2}. *Biophys. J.* 69:2623–41
33. Duguid JG, Bloomfield VA, Benevides JM, Thomas GJ Jr. 1996. DNA melting investigated by differential scanning calorimetry and Raman spectroscopy. *Biophys. J.* 71: 3350–60
34. Goldstein SR, Kidder LH, Herne TM, Levin IW, Lewis EN. 1996. The design and implementation of a high-fidelity Raman imaging microscope. *J. Microsc.* 184:35–45
35. Greve J, Puppels GJ. 1993. Raman microspectroscopy of single whole cells. In *Advances in Spectroscopy (Biomolecular Spectroscopy)*, ed. RJH Clark, RE Hester, 20A:55–127. New York: Wiley & Sons. 383 pp.
36. Hashimoto S, Ikeda T, Takeuchi H, Harada I. 1993. Utilization of a prism monochromator as a sharp-cut bandpass filter in ultraviolet Raman spectroscopy. *Appl. Spectrosc.* 47:1283–85
37. Hudson BS, Mayne LC. 1987. Peptides and protein side chains. In *Biological Applications of Raman Spectroscopy (Resonance Raman Spectra of Polyenes and Aromatics)*, ed. TG Spiro, 2:181–209. New York: Wiley & Sons. 367 pp.
38. Jayaraman V, Rodgers KR, Mukerji I, Spiro TG. 1995. Hemoglobin allostery: resonance Raman spectroscopy of kinetic intermediates. *Science* 269:1843–48
39. Kincaid JR. 1995. Structure and dynamics of transient species using time-resolved resonance Raman spectroscopy. In *Methods in Enzymology*, ed. K Sauer, 246:460–500. New York: Academic. 816 pp.
40. Kraulis PJ. 1991. MOLSCRIPT. *J. Appl. Crystallogr.* 24:946–50
41. Laporte L, Thomas GJ Jr. 1998. Structural basis of DNA recognition and mechanism of quadruplex formation by the β-subunit of the *Oxytricha* telomere binding protein. *Biochemistry* 37:1327–35
42. Laporte L, Thomas GJ Jr. 1998. A hairpin conformation for the 3′ overhang of *Oxytricha nova* telomeric DNA. *J. Mol. Biol.* 281:261–70
43. Laporte L, Thomas GJ Jr. 1999. Molecular mechanism of DNA recognition by the α-subunit of the *Oxytricha* telomere binding protein. *Biochemistry.* In press
44. Li H, Thomas GJ Jr. 1991. Cysteine conformation and sulfhydryl interactions in proteins and viruses. I. Correlation of the Raman S-H band with hydrogen bonding and intramolecular geometry in model compounds. *J. Am. Chem. Soc.* 113:456–62
45. Li T, Johnson JE, Thomas GJ Jr. 1993. Raman dynamic probe of hydrogen exchange in bean pod mottle virus: base-specific retardation of exchange in packaged ssRNA. *Biophys. J.* 65:1963–72
46. Luisi B. 1995. DNA-protein interaction at high resolution. In *DNA-Protein: Structural Interactions*, ed. DMJ Lilley, pp. 1–48. Oxford: IRL
47. Manoharan R, Wang Y, Feld MS. 1996. Histochemical analysis of biological tissues using Raman spectroscopy. *Spectrochim. Acta* 52A:215–49
48. Marvin DA. 1998. Filamentous phage structure, infection and assembly. *Curr. Opin. Struct. Biol.* 8:150–58
49. Marvin DA, Hale RD, Nave C, Helmer Citterich M. 1994. Molecular models and structural comparisons of native and mutant class I filamentous bacteriophages Ff (fd, f1, M13), If1 and IKe. *J. Mol. Biol.* 235:260–86
50. Matsuno M, Takeuchi H, Overman SA, Thomas GJ Jr. 1998. Orientations of tyrosines 21 and 24 in coat subunits of *Ff* filamentous virus: determination by

Annu. Rev. Biophys. Biomol. Struct. 1999.28:1-27. Downloaded from www.annualreviews.org
by Harvard University on 01/12/12. For personal use only.

Raman linear intensity difference spectroscopy and implications for subunit packing. *Biophys. J.* 74:3217–25
51. Miura T, Benevides JM, Thomas GJ Jr. 1995. A phase diagram for sodium and potassium ion control of polymorphism in telomeric DNA. *J. Mol. Biol.* 248:233–38
52. Miura T, Thomas GJ Jr. 1994. Structural polymorphism of telomeric DNA: interquadruplex and duplex-quadruplex conversions probed by Raman spectroscopy. *Biochemistry* 33:7848–56
53. Miura T, Thomas GJ Jr. 1995. Structure and dynamics of interstrand guanine association in quadruplex telomeric DNA. *Biochemistry* 34:9645–54
54. Miura T, Thomas GJ Jr. 1995. Raman spectroscopy of proteins and their assemblies. In *Subcellular Biochemistry (Proteins: Structure, Function and Engineering)*, ed. BB Biswas, S Roy, 24:55–99. New York: Plenum. 436 pp.
55. Miura T, Thomas GJ Jr. 1995. Optical and vibrational spectroscopic methods. In *Introduction to Biophysical Methods for Protein and Nucleic Acid Research*, ed. JA Glasel, MP Deutscher, pp. 261–315. New York: Academic. 510 pp.
56. Nabiev IR, Sokolov KV, Manfait M. 1993. Surface-enhanced Raman spectroscopy and its biomedical applications. In *Advances in Spectroscopy (Biomolecular Spectroscopy)*, ed. RJH Clark, RE Hester, 20A:267–338. New York: Wiley & Sons. 383 pp.
57. Nafie LA. 1996. Vibrational optical activity. *Appl. Spectrosc.* 50:14A–26A
58. Nishimura Y, Hirakawa AY, Tsuboi M. 1978. Resonance Raman spectroscopy of nucleic acids. In *Advances in Infrared and Raman Spectroscopy*, ed. RJH Clark, RE Hester, 5:217–75. London: Heyden. 405 pp.
59. Overman SA, Aubrey KL, Vispo NS, Cesareni G, Thomas GJ Jr. 1994. Novel tyrosine markers in Raman spectra of wild-type and mutant (Y21M and Y24M) *Ff* virions indicate unusual environments for coat protein phenoxyls. *Biochemistry* 33:1037–42
60. Overman SA, Thomas GJ Jr. 1995. Raman spectroscopy of the filamentous virus *Ff* (*fd, f1, M13*): structural interpretation for coat protein aromatics. *Biochemistry* 34:5440–51
61. Overman SA, Thomas GJ Jr. 1998. Novel vibrational assignments for proteins from Raman spectra of viruses. *J. Raman Spectrosc.* 29:23–29
62. Overman SA, Thomas GJ Jr. 1998. Amide modes of the α-helix: Raman spectroscopy of filamentous virus *fd* containing peptide ^{13}C and ^{2}H labels in coat protein subunits. *Biochemistry* 37:5654–65
63. Overman SA, Tsuboi M, Thomas GJ Jr. 1996. Subunit orientation in the filamentous virus *Ff* (*fd, f1, M13*). *J. Mol. Biol.* 259:331–36
64. Peticolas WL. 1995. Raman spectroscopy of DNA and proteins. In *Methods in Enzymology*, ed. K Sauer, 246:389–416. New York: Academic. 816 pp.
65. Prasad BVV, Prevelige PE, Marietta E, Chen RO, Thomas D, et al. 1993. Three-dimensional transformation of capsids associated with genome packaging in a bacterial virus. *J. Mol. Biol.* 231:65–74
66. Prevelige PE Jr, King J. 1993. Assembly of bacteriophage P22: a model for ds-DNA virus assembly. *Prog. Med. Virol.* 40:206–21
67. Prevelige PE, Thomas D, Aubrey KL, Towse SA, Thomas GJ Jr. 1993. Subunit conformational changes accompanying bacteriophage *P22* capsid maturation. *Biochemistry* 32:537–43
68. Puppels GJ, van Rooijen M, Otto C, Greve J. 1993. Confocal Raman microspectroscopy. In *Fluorescent and Luminescent Probes for Biological Activity*, ed. WT Mason, pp. 237–58. New York: Academic
69. Raman CV, Krishnan KS. 1928. A new class of spectra due to secondary radiation, Part I. *Indian J. Phys.* 2:399–419
70. Reilly KE, Thomas GJ Jr. 1994. Hydrogen exchange dynamics of the *P22* virion determined by time-resolved Raman spectroscopy: effects of chromosome packaging on the kinetics of nucleotide exchanges. *J. Mol. Biol.* 241:68–82
71. Rodgers KR, Spiro TG. 1994. Nanosecond dynamics of the R $\rightarrow$ T transition in hemoglobin: ultraviolet Raman studies. *Science* 265:1697–99
72. Rousseau DL. 1981. Raman difference spectroscopy as a probe of biological molecules. *J. Raman Spectrosc.* 10:94–99
73. Russell MP, Vohník S, Thomas GJ Jr. 1996. Design and performance of an ultraviolet resonance Raman spectrometer for proteins and nucleic acids. *Biophys. J.* 68:1607–12
74. Sen D, Gilbert W. 1988. Formation of parallel four-stranded complexes by guanine-rich motifs for meiosis. *Nature* 334:364–66
75. Sen D, Gilbert W. 1990. A sodium-potassium switch in the formation of four-stranded G4-DNA. *Nature* 344:410–14
76. Sijtsema NM, Wouters SD, de Grauw C, Otto C, Greve J. 1998. Confocal direct imaging Raman microscope: design and

Annu. Rev. Biophys. Biomol. Struct. 1999.28:1-27. Downloaded from www.annualreviews.org
by Harvard University on 01/12/12. For personal use only.

applications in biology. *Appl. Spectrosc.* 52:348–55
77. Spiro TG, Czernuszewicz RS. 1995. Resonance Raman spectroscopy of metalloproteins. In *Methods in Enzymology*, ed. K Sauer, 246:416–60. New York: Academic. 816 pp.
78. Steitz TA. 1990. Structural studies of protein-nucleic acid interactions. *Q. Rev. Biophys.* 23:205–80
79. Symmons MF, Welsh LC, Nave C, Marvin DA, Perham RN. 1995. Matching electrostatic charge between DNA and coat protein in filamentous bacteriophage. Fibre diffraction of charge-deletion mutants. *J. Mol. Biol.* 245:86–91
80. Takeuchi H, Matsuno M, Overman SA, Thomas GJ Jr. 1996. Raman linear intensity difference of flow-oriented macromolecules: orientation of the indole ring of tryptophan 26 in filamentous virus *fd*. *J. Am. Chem. Soc.* 118:3498–507
81. Thomas GJ Jr. 1986. Applications of Raman spectroscopy in structural studies of viruses, nucleoproteins and their constituents. In *Advances in Spectroscopy (Spectroscopy of Biological Systems)*, ed. RJH Clark, RE Hester, 13:233–309. London: Wiley & Sons. 547 pp.
82. Thomas GJ Jr, Benevides JM, Overman SA, Ueda T, Ushizawa K, et al. 1995. Polarized Raman spectra of oriented fibers of *A* DNA and *B* DNA: anisotropic and isotropic local Raman tensors of base and backbone vibrations. *Biophys. J.* 68:1073–88
83. Thomas GJ Jr, Murphy P. 1975. Structure of coat proteins in *Pf1* and *fd* virions by laser Raman spectroscopy. *Science* 188:1205–7
84. Thomas GJ Jr, Prescott B, Day LA. 1983. Structure similarity, difference and variability in the filamentous viruses *fd*, *If1*, *IKe*, *Pf1*, *Xf* and *Pf3*. *J. Mol. Biol.* 165:321–56
85. Thomas GJ Jr, Prescott B, Opella SJ, Day LA. 1988. Sugar pucker and phosphodiester conformations in viral genomes of filamentous bacteriophages: *fd*, *If1*, *IKe*, *Pf1*, *Xf* and *Pf3*. *Biochemistry* 27:4350–57
86. Thomas GJ Jr, Tsuboi M. 1993. Raman spectroscopy of nucleic acids and their complexes. *Adv. Biophys. Chem.* 3:1–70
87. Thomas GJ Jr, Wang AHJ. 1988. Laser Raman spectroscopy of nucleic acids. *Nucleic Acids Mol. Biol.* 2:1–30
88. Tonge PJ, Carey PR. 1993. Raman, resonance Raman and FTIR spectroscopic studies of enzyme-substrate complexes. In *Advances in Spectroscopy (Biomolecular Spectroscopy)*, ed. RJH Clark, RE Hester, 20A:129–61. New York: Wiley & Sons. 383 pp.
89. Tsuboi M, Ikeda T, Ueda T. 1991. Raman microscopy of a small uniaxial crystal: tetragonal aspartame. *J. Raman Spectrosc.* 22:619–26
90. Tsuboi M, Nishimura Y, Hirakawa AY. 1987. Resonance Raman spectroscopy and normal modes of the nucleic acid bases. In *Biological Applications of Raman Spectroscopy (Resonance Raman Spectra of Polyenes and Aromatics)*, ed. TG Spiro, 2:109–79. New York: Wiley & Sons. 367 pp.
91. Tsuboi M, Overman SA, Thomas GJ Jr. 1996. Orientation of tryptophan 26 in coat protein subunits of the filamentous virus *Ff* by polarized Raman microspectroscopy. *Biochemistry* 35:10403–10
92. Tsuboi M, Thomas GJ Jr. 1997. Raman scattering tensors in biological molecules and their assemblies. *Appl. Spectrosc. Rev.* 32:263–99
93. Tuma R, Prevelige PE Jr, Thomas GJ Jr. 1996. Structural transitions in the scaffolding and coat proteins of P22 virus during assembly and disassembly. *Biochemistry* 35:4619–27
94. Tuma R, Prevelige PE Jr, Thomas GJ Jr. 1998. Mechanism of capsid maturation in a double-stranded DNA virus. *Proc. Natl. Acad. Sci. USA* 95:9885–90
95. Tuma R, Thomas GJ Jr. 1996. Theory, design and characterization of a microdialysis flow cell for Raman spectroscopy. *Biophys. J.* 71:3454–66
96. Tuma R, Thomas GJ Jr. 1997. Mechanism of virus assembly probed by Raman spectroscopy: the icosahedral bacteriophage P22. *Biophys. Chem.* 68:17–31
97. Wen ZQ, Overman SA, Thomas GJ Jr. 1997. Structure and interactions of the single-stranded DNA genome of filamentous virus *fd*. Investigation by ultraviolet resonance Raman spectroscopy. *Biochemistry* 36:7810–20

Annual Review of Biophysics and Biomolecular Structure
Volume 28, 1999

CONTENTS

Annu. Rev. Biophys. Biomol. Struct. 1999.28:1-27. Downloaded from www.annualreviews.org
by Harvard University on 01/12/12. For personal use only.